Chemical Science

EDGE ARTICLE

View Article Online
View Journal | View Issue

Cite this: *Chem. Sci.*, 2019, **10**, 1619

All publication charges for this article have been paid for by the Royal Society of Chemistry

In situ imaging of aminopeptidase N activity in hepatocellular carcinoma: a migration model for tumour using an activatable two-photon NIR fluorescent probe†

Haidong Li,[a] Yueqing Li,[b] Qichao Yao,[a] Jiangli Fan,*[ad] Wen Sun,[ad] Saran Long,[ad] Kun Shao,[ad] Jianjun Du,[a] Jingyun Wang[cd] and Xiaojun Peng[ad]

Received 21st October 2018
Accepted 25th November 2018

DOI: 10.1039/c8sc04685a

rsc.li/chemical-science

CD13/aminopeptidase N (APN), which is a zinc-dependent metalloproteinase, plays a vital role in the growth, migration, angiogenesis, and metastasis of tumours. Thus, *in situ* molecular imaging of endogenous APN levels is considerably significant for investigating APN and its different functions. In this study, a novel two-photon near-infrared (NIR) fluorescence probe **DCM-APN** was prepared to perform *in vitro* and *in vivo* tracking of APN. The *N*-terminal alanyl site of probe **DCM-APN** was accurately hydrolysed to the amino group, thereby liberating strong fluorescence owing to the recovery of the Intramolecular Charge Transfer (ICT) effect. By considering its outstanding selectivity, ultra-sensitivity (DL 0.25 ng mL^{-1}) and favourable biocompatibility, the probe **DCM-APN** was used to distinguish between normal cells (LO2 cells) and cancer cells (HepG-2 and B16/BL6 cells). Furthermore, migration of hepatocellular carcinoma cells was apparently inhibited by ensuring that the APN catalytic cavity was occupied by bestatin. The identification of three-dimensional (3D) fluorescence in cancer tissues was completed under two-photon excitation coupled with lighting up hepatocellular carcinoma tumours *in situ*; this revealed that probe **DCM-APN** is an effective tool for detecting APN, thereby assisting in the early diagnosis of tumour in clinical medicine.

Introduction

Aminopeptidase N (APN/CD13, EC 3.4.11.2), also known as a dimeric membrane protein and a member of the zinc metallopeptidase family,[1,2] participates in many physiological and pathological processes, including signal transduction, neuropeptide degradation, immunological responses, and antigen processing.[3] APN has been extensively considered to be a marker for hematopoietic cells of myeloid origin, which facilitates the classification of human leukaemia cells through its antigenicity.[4] Because APN plays a vital role in tumour invasion, angiogenesis, and metastasis,[5] if an elevated APN is observed above a threshold, it could be employed as a cancer biomarker for assessing a patient and diagnosing clinical cancer.[6–8] Therefore, developing valid methods that can be employed to track the activity of APN is considered to be of great medical significance.[9–12]

To date, fluorescence imaging has been extensively employed to visualize biologically significant analytes as well as to perform image-guided surgery because of its high selectivity, sensitivity, and spatial and temporal resolutions, especially in a noninvasive manner.[13–23] Specifically, the probes that utilize near-infrared (NIR) emission (650–900 nm) fluorescence are highly favoured for application in bio-imaging because they exhibit the ability to overcome issues such as tissue penetration and autofluorescence.[24–26] In addition, two-photon fluorescence microscopy (under an excitation of 700–1000 nm) provides a satisfactory cell and tissue imaging solution that can be attributed to the advantages of two-photon technology, including long wavelength excitation, minimal photo-damage, and deep tissue penetration.[27–32] To date, only one NIR fluorescence probe has been reported from among the few fluorescence probes employed for the detection of APN.[4,33,34] Unfortunately, severe cross-talk between the excitation and emission spectra[4] weakens its capability of gathering a valid signal.[35] Furthermore, to the best of our knowledge, a two-photon fluorescence probe has not been developed for tracking APN activity in both living cells and tissues.

[a]*State Key Laboratory of Fine Chemicals, Dalian University of Technology, 2 Linggong Road, Dalian 116024, P. R. China. E-mail: fanjl@dlut.edu.cn*

[b]*School of Pharmaceutical Science and Technology, Dalian University of Technology, 2 Linggong Road, Hi-tech Zone, Dalian 116024, P. R. China*

[c]*School of Life Science and Biotechnology, Dalian University of Technology, 2 Linggong Road, Dalian 116024, P. R. China*

[d]*Research Institute of Dalian University of Technology in Shenzhen, Gaoxin South fourth Road, Nanshan District, Shenzhen 518057, China*

† Electronic supplementary information (ESI) available. See DOI: 10.1039/c8sc04685a

In this work, we report a novel NIR two-photon fluorescence probe **DCM-APN** for detecting APN by combining L-alanine as the recognition unit with the classical dicyanomethylene-benzopyran (DCM) fluorophores. **DCM-APN** was transformed into DCM-NH_2 by performing enzymatic hydrolysis of the amide bond of APN, thereby releasing the bare amino group as a strong electron donor and liberating the NIR fluorescence signal at 664 nm based on the enhanced intramolecular charge transfer (ICT) effect. Notably, a large Stokes shift of $\Delta\lambda = 194$ nm ($\lambda_{abs} = 470$ nm; $\lambda_{em} = 664$ nm) considerably enhanced the ability to collect valid signals. Furthermore, **DCM-APN** was employed to distinguish normal cells from cancer cells as well as normal liver tissue from hepatocellular carcinoma tissue *via* three-dimensional (3D) imaging using a two-photon excitation fluorescence process. The *in vivo* transplanted tumour in nude BALB/c mice imaging revealed that the activatable probe **DCM-APN** can be a promising tool to study APN activity.

Results and discussion

Design and synthesis of probe DCM-APN

Dicyanomethylene-benzopyran (DCM) fluorophores possess an inherently classic donor–π–acceptor (D–π–A) structure,[36–38] and have been extensively employed in the field of fluorescence probes because of their excellent photo-stability, broad absorption bands, controllable emission spectrum, large Stokes shift and considerable two-photon absorption cross-section.[27] Researchers have found that alanine decorated ligands are preferred by APN within accessible catalytic cavities.[1] Hence, by conjugating the bare amine group of DCM-NH_2 with L-alanine's carboxyl (*i.e.* potential recognition sites), an enzyme-triggered two-photon fluorescent probe **DCM-APN** was successfully synthesized as illustrated in Scheme S1,† which was accurately validated using nuclear magnetic resonance (NMR) spectroscopy and high resolution mass spectrometry (ESI-HRMS), as presented in the ESI.†

Spectroscopic characteristics and response to APN

The spectral properties of probe **DCM-APN** were investigated in aqueous solution (PBS/DMSO = 7 : 3, v/v, 0.01 M, pH = 7.4). As depicted in Fig. 1a, with an increase in the concentration of APN (0–200 ng mL^{-1}), there is an obvious 28 nm red-shift in absorption profiles ranging from 442 nm to 470 nm (an evident isosbestic point at around 458 nm) that is accompanied by an evident color change of the solution from pale yellow to light red (Fig. S1†). Simultaneously, the fluorescence intensity of probe **DCM-APN** (10 μM, $\phi = 0.6\%$) at approximately 664 nm was observed to gradually increase owing to the fact that APN specifically cuts the amide bond in the aqueous buffer solution (Fig. 1b and S2†), thereby releasing the NIR fluorescence signal of DCM-NH_2 ($\phi = 2.8\%$, Scheme 1). Notably, a large Stokes shift of $\Delta\lambda = 194$ nm considerably reduced the interference of background noise and significantly improved the accuracy of detection (Fig. 1c). Furthermore, a linear functional relationship ($R^2 = 0.999$) was obtained at the fluorescence intensity of 664 nm, and a low dose enzyme concentration (0–100 ng mL^{-1}) with a detection limit for APN as low as 0.25 ng mL^{-1} (Fig. 1d) (based on the $3\sigma/k$ principle) clearly indicates that probe **DCM-APN** could be used to quantitatively identify trace amounts of APN *in vitro*.

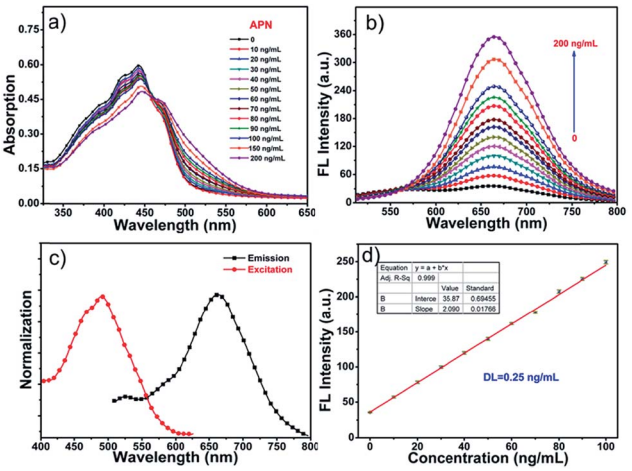

Fig. 1 (a) UV-vis absorption and (b) fluorescence titration experiments of probe **DCM-APN** (10 μM) at various APN concentrations (titration concentrations of 0–200 ng mL^{-1}) in aqueous solution (PBS/DMSO = 7 : 3, v/v, 0.01 M, pH = 7.4). (c) Normalization excitation and emission spectra of probe **DCM-APN** (10 μM) with 100 ng mL^{-1} APN in aqueous solution. (d) Linear relationship between the fluorescence intensity (664 nm) and various concentrations of APN (0–100 ng mL^{-1}). The experiments were repeated thrice and the data were obtained as the mean (±S.D.). $\lambda_{ex} = 490$ nm, slit: 10/10 nm.

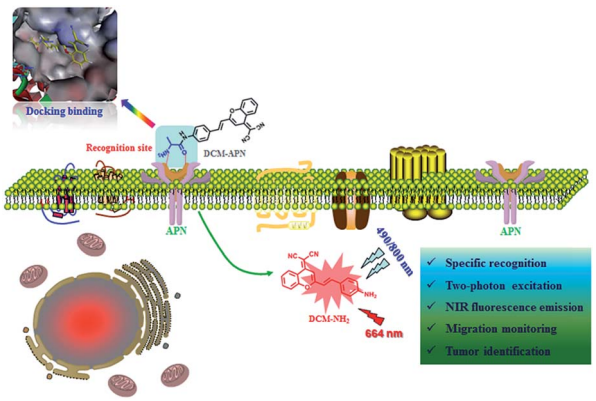

Scheme 1 The recognition mechanism of probe **DCM-APN** towards APN.

Response speed and selectivity

The fluorescence intensities of probe **DCM-APN** (10 μM) around 664 nm were periodically recorded in the presence of 100 ng mL^{-1} APN at 37 °C in aqueous solution. The enzymatic reaction was complete in approximately 120 min (Fig. 2a) compared to that in the absence of APN (Fig. S3†). Good specificity is one of the key indicators for evaluating probe usability in a complex bio-system. Subsequently, the influence of common biological interferents towards probe **DCM-APN** including ions (Na^+; K^+;

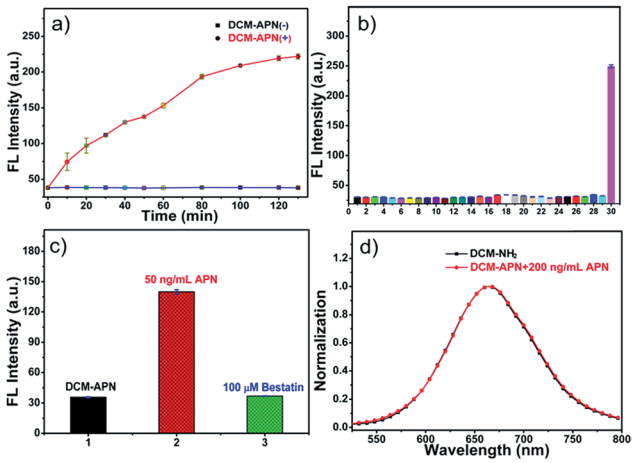

Fig. 2 (a) Time response of probe **DCM-APN** *versus* APN. (b) Fluorescence intensity ($F_{664\ nm}$) changes of probe **DCM-APN** (10 μM) for different analytes in aqueous solution (PBS/DMSO = 7 : 3, v/v, 0.01 M, pH = 7.4). Except for special statement, the concentration of other interferents was 500 μM, inset (1): blank; (2): Na^+; (3): K^+; (4): Ca^{2+}; (5): Ni^{2+}; (6): Mg^{2+}; (7): NH_4^+; (8): F^-; (9): Cl^-; (10): Br^-; (11): I^-; (12): CH_3COO^-; (13): HCO_3^-; (14): CO_3^{2-}; (15): S^{2-}; (16): HPO_4^-; (17): NO_3^-; (18): SO_4^{2-}; (19): SCN^-; (20): NO_2^-; (21): glutathione (GSH); (22): cysteine (Cys); (23): homocysteine (Hcy); (24): ascorbic acid (AA); (25): NO; (26): H_2O_2 (100 μM); (27): nitroreductase (10 μg mL^{-1}); (28) transglutaminase (60 mU mL^{-1}); (29): γ-GGT (300 ng mL^{-1}) (30): APN (100 ng mL^{-1}). (c) Inhibition tests of probe **DCM-APN** (10 μM) for APN. (d) Normalization merged spectra of probe **DCM-APN** pretreated with APN and DCM-NH_2 intermediate. The experiments were repeated thrice and the data are denoted as mean (±S.D.). λ_{ex} = 490 nm, slit: 10/10 nm.

Ca^{2+}; Mg^{2+}; Ni^{2+}; NH_4^+; F^-; Cl^-; Br^-; I^-; CH_3COO^-; HCO_3^-; CO_3^{2-}; S^{2-}; HPO_4^-; NO_3^-; SO_4^{2-}; SCN^-; NO_2^-), amino acids (glutathione; cysteine; homocysteine), redox species (ascorbic acid; H_2O_2; NO) and related-enzymes (nitroreductase; transglutaminase; γ-glutamyltranspeptidase) was investigated. As depicted in Fig. 2b and S4,† only APN caused obvious fluorescence enhancement as it has the ability to specifically catalyze the conversion of the amide linkage of **DCM-APN** to the DCM fluorophore, thereby verifying that probe **DCM-APN** possesses excellent selectivity with respect to APN.

Micro-environmental influence

The influence of micro-environmental conditions, including pH and temperature, was investigated. As shown in Fig. S5,† the probe **DCM-APN** (10 μM) exhibited good stability at different pH values ranging from 4.75 to 10.27. Temperature had little effect on the probe itself ranging from 25 °C to 50 °C (Fig. S6a†) and the fluorescence intensity of probe **DCM-APN** towards APN around 664 nm increased a maximum at 37 °C (Fig. S6b†). Based on the above results, the probe **DCM-APN** shows excellent performance during the recognition of APN under normal physiological conditions.

Sensing mechanism

In order to explore the sensing mechanism of probe **DCM-APN** towards APN, the high resolution mass spectra of the resulting catalytic product were initially recorded (Fig. S7†). Here, a distinct peak was observed at m/z = 312.1136, which was consistent with the positive ion mode of DCM-NH_2 (calcd. 312.1131 for $[M + H]^+$). Additionally, normalization fluorescence spectra of DCM-NH_2 along with those of the catalytic product completely coincided with their excitation and emission spectra (Fig. 1c, 2d and S8†). This further verifies that APN exhibits the ability to catalyze substrate sites (as per Scheme 1). Furthermore, when pretreated using 100 μM bestatin (an inhibitor of APN) in aqueous solution, the activity of APN was found to be completely suppressed (Fig. 2c and S9†) because its active sites were occupied by bestatin.

To obtain further details related to the interactions between probe **DCM-APN** and APN, molecular docking investigations based on Accelrys' Discovery Studio 2.5 platform were conducted. The X-ray crystal structure of human APN that was measured at a resolution of 1.35095 Å using amastatin (PDB: 4FYT) from the RCSB PDB database was employed. In the crystal, a zinc ion was chelated by three ligands that were provided by His388, His392 and Glu411 in the catalytic center of APN (Fig. S10†). After defining the binding sphere and molecular docking parameters (Fig. 3a), probe **DCM-APN** was docked with APN and it could easily reach the coordination center of zinc ion, which could be ascribed to the hydrophobic interaction with the *N*-terminal amino acid of peptides (Fig. S11†). Furthermore, the coordinate bond lengths in **DCM-APN** and the zinc ion were 2.117 Å and 2.256 Å (Fig. 3b), respectively, and were close to the other three bond lengths observed in APN (2.027 Å, 2.085 Å and 1.936 Å, Fig. S10†). In addition, the interactions of the existing hydrogen bonds between probe **DCM-APN** and other peptides, such as Glu355, Glu411, Ala353 and Tyr477, firmly anchor the *N*-terminal amine of probe **DCM-APN** to the active catalytic site (Fig. 3c). Therefore, using water as the catalyst, the scissile amide bond of probe **DCM-APN** was precisely hydrolyzed in the catalytic system that was centered on the zinc ions. Simultaneously, DCM-NH_2 was released with enhanced NIR fluorescence emission. To our delight, the results of the docking simulation agreed well with those of the aforementioned experimental phenomena, which completely confirmed the response of probe **DCM-APN** to APN.

Cytotoxicity and cell imaging

To evaluate the biocompatibility of the probe, the viability of HepG-2 cells (cancer cells) and LO2 cells (normal cells) towards

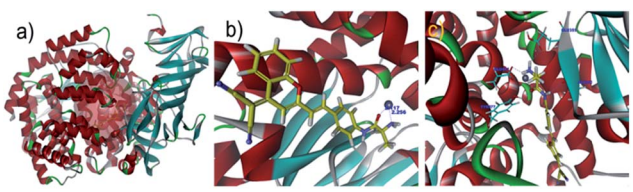

Fig. 3 (a) Stereo image of human APN with a binding location (red transparent sphere). (b) Coordination mode of probe **DCM-APN** with a zinc ion in the hydrophobic cavity. (c) Hydrogen bonds between probe **DCM-APN** and APN. The zinc ion is identified by the grey ball. All carbon atoms of probe **DCM-APN** are indicated in yellow.

various doses of probe **DCM-APN** (0–10 μM) was measured using standard 5-diphenyltetrazolium bromide (MTT) assays for 24 h. The experimental results are demonstrated in Fig. S12 and S13,† which reveal the considerably low cytotoxicity of the probe.

Subsequently, hepatoma carcinoma cells (HepG-2 cells, APN+) and mouse melanoma (B16/BL6 cells, APN+) were selected to monitor the endogenous APN activity on the surfaces of cell membranes.[5,10] Compared to the LO2 cells with a low APN expression (Fig. 4q),[34] the NIR fluorescence signal was obtained (Fig. 4e) after the HepG-2 cells were treated with 2.5 μM probe **DCM-APN** for 10 min. The same features were present in B16/BL6 cells (Fig. S14†), which were ascribed to the enzymatic hydrolysis of the probe in cells exhibiting abnormal APN activity. With a prolonged incubation time, the fluorescence intensity of the cell continued to increase (Fig. S15 and S16†). Then, when incubated with 50 μM bestatin (the inhibitor of APN) for 2 h, a significant reduction in the fluorescence intensity of HepG-2 cells could be observed (Fig. 4h). To clearly quantify the results, the fluorescence intensity values were measured using an average of nine regions of interest (ROIs) obtained from various treated cells (Fig. 4v). As observed in Fig. 4j–l, high resolution two-photon imaging of probe **DCM-APN** in living HepG-2 cells was also obtained and compared with that in Fig. S17,† which further established that probe **DCM-APN** could be employed to track endogenous APN activity *in situ* using a two-photon platform. Additionally, the cell morphology and fluorescence intensity of ROIs (Fig. S18a and b†) were observed to remain unchanged (Fig. S18d†) after continuous two-photon irradiation at 800 nm for 1000 s, which confirmed that probe **DCM-APN** exhibited high photo-stability. Therefore, probe **DCM-APN** might be employed to distinguish cancer cells from normal cells *via* imaging techniques.

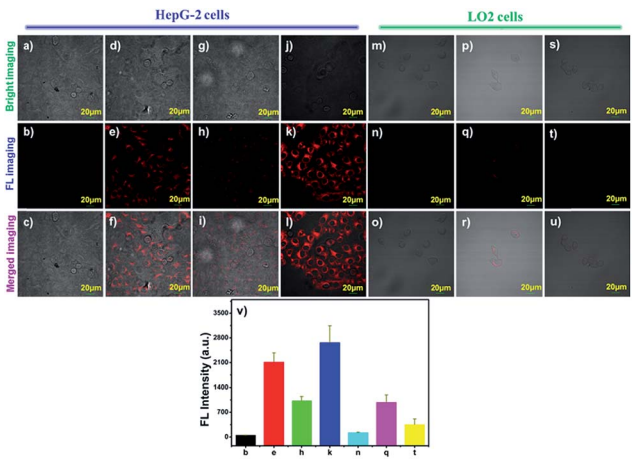

Fig. 4 Fluorescence imaging of probe **DCM-APN** in living cells. (a–c) As-received HepG-2 cells; (d–f) HepG-2 cells treated with 2.5 μM of probe **DCM-APN**; (g–i) HepG-2 cells pre-incubated with 50 μM bestatin with the addition of 2.5 μM of probe **DCM-APN**; (j–l) two-photon fluorescence images of the HepG-2 cells treated with 2.5 μM of probe **DCM-APN**; (m–o) as-received LO2 cells; (p–r) LO2 cells incubated with 2.5 μM of probe **DCM-APN**; (s–u) LO2 cells pre-treated with 50 μM bestatin with the addition of 2.5 μM of probe **DCM-APN**; (v) the NIR fluorescence intensities were recorded by averaging the nine regions of interest (ROIs) from various treated cells (b, e, h, k, n, q and t). Error bar = RSD (n = 9). One-photon mode: λ_{ex} = 488 nm and λ_{em} = 610–660 nm; two-photon mode: λ_{ex} = 800 nm and λ_{em} = 575–630 nm. Scale bar = 20 μm.

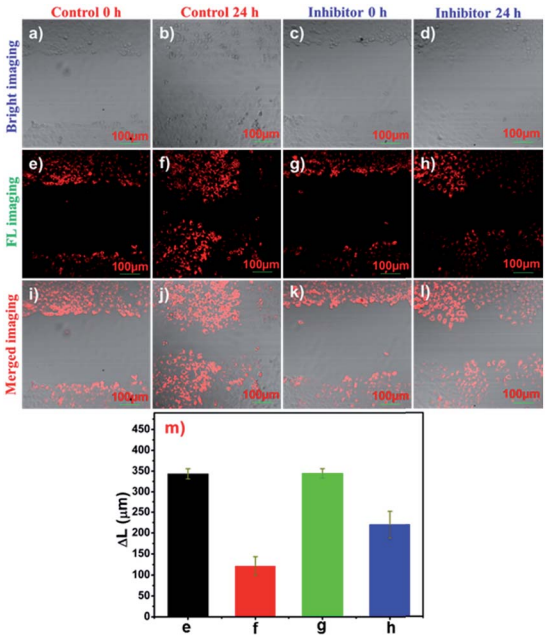

Fig. 5 Cell motility assays of probe **DCM-APN** in HepG-2 cells. The cellular morphology of HepG-2 (a, c, e, g, i, and k) before and after a 24 h injury (control: b, f, and j; with 100 μM bestatin: d, h, and l). (m) The distance (ΔL) of wounds obtained from (e–h). Error bar = RSD (n = 11). λ_{ex} = 488 nm and λ_{em} = 610–660 nm. Scale bar = 20 μm.

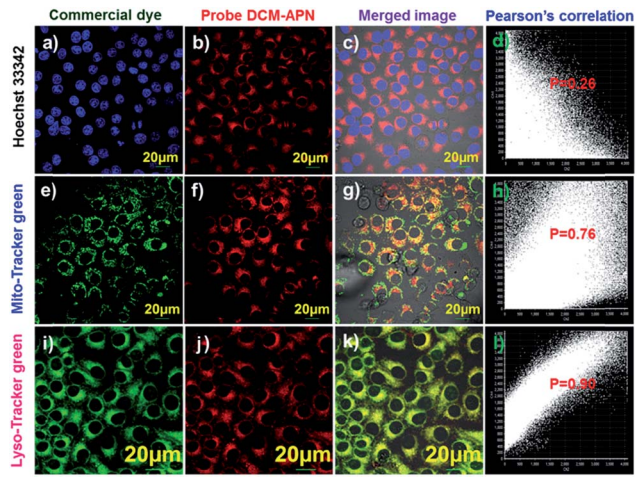

Fig. 6 Subcellular localization experiments in living HepG-2 cells. (a, e and i) Commercial Hoechst 33342 (λ_{ex} = 405 nm, λ_{em} = 410–480 nm), Mito-Tracker dye (λ_{ex} = 488 nm, λ_{em} = 500–560 nm), and Lyso-Tracker dye (λ_{ex} = 488 nm, λ_{em} = 500–560 nm) channels, respectively; (b, f and g) the NIR channel of probe **DCM-APN** (λ_{ex} = 488 nm, λ_{em} = 610–660 nm); (c, g and k) the merged channel; (d, h and l) Pearson's correlation. Scale bar = 20 μm.

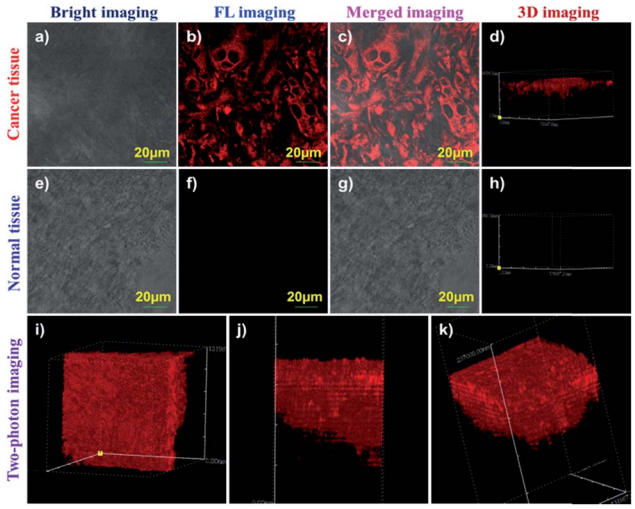

Fig. 7 One/two-photon fluorescence imaging of the endogenous APN activity within various tissues. The one-photon mode (λ_{ex} = 488 nm and λ_{em} = 610–660 nm): (a–d) hepatocellular carcinoma tissue; (e–h) normal liver tissue; the two-photon mode (λ_{ex} = 800 nm and λ_{em} = 575–630 nm): (i–k) 3D fluorescence imaging of hepatocellular carcinoma tissue. Scale bar = 20 μm.

Cell motility assays

Tumour cell migration is of crucial importance for the rapid tumour progression and cancer treatment in clinical medicine. Correspondingly, aminopeptidases play a vital role in the angiogenesis, metastasis, and migration of a solid tumour.[2,39,40] To visualize the APN activity in the migration of tumour cells, cell motility assays were observed. Living HepG-2 cells were obtained immediately after an injury within 350 μm (Fig. 5e and g). After the cells were cultured for 24 h by conducting pre-treatment using bestatin (100 μM) at 37 °C, their horizontal migration was observed to be remarkably inhibited (Fig. 5h). In comparison, the migration of the HepG-2 cells was visible in the control group (Fig. 5f). The migration distances are depicted in Fig. 5m and they indicated that APN participated in the regulation of tumour migration. Therefore, the treatment of metastatic tumours may benefit from APN inhibitor addition strategies for patients as an adjuvant therapy.

Subcellular localization

Co-localization experiments were performed to explore the distribution of probe **DCM-APN** in living cells. High purity commercial Hoechst 33342 (Fig. 6a), Mito-Tracker (Fig. 6e), and Lyso-Tracker (Fig. 6i) were co-incubated with probe **DCM-APN** (Fig. 6b, f and j) in HepG-2 cells. The NIR channel (Fig. 6j) overlaid well with the Lyso-Tracker channel (Fig. 6i) and resulted in a Pearson's correlation coefficient of 0.90 (Fig. 6l), which was higher than that of the nucleus (P = 0.26, Fig. 6d) and mitochondria (P = 0.76, Fig. 6h). The results are consistent with those of the B16/BL6 cells (Fig. S19†), demonstrating that probe **DCM-APN** mainly clustered as lysosomes. We inferred that lysosome labelling in this manner could be attributed to the alkalization effect of the bare amino products of DCM-NH_2 (Scheme 1).

Imaging of endogenous APN activity in tissues

To the best of our knowledge, until now, there has been no fluorescence probe capable of monitoring APN in different tissues for clinical diagnosis. Therefore, we prepared various tissues from hepatocellular carcinoma tissue and normal liver tissue using a LEICA CM1860 UV clinical cryostat to verify probe **DCM-APN**. As depicted in Fig. 7a–d, 20 μm of cancer tissue from bare BABL/c mice bearing HepG-2 xenograft tumours demonstrated a strong fluorescence signal (Fig. 7c), with 2.5 μM of probe **DCM-APN** for 30 min. In sharp contrast, no fluorescence signal was measured from the normal liver tissue that was pre-incubated with 2.5 μM of probe **DCM-APN** (Fig. 7g). Additionally, the 3D fluorescence imaging results of tissues (Fig. 7d and h) were in contrast, which proved that the probe **DCM-APN** is an effective tool for oncologists in medical diagnosis of cancer. Considering deep tissue penetration under two-photon excitation,[27] as depicted in Fig. 7i–k, 3D imaging of 200 μm of hepatocellular carcinoma tissue treated with 5 μM of probe **DCM-APN** resulted in the production of a remarkable fluorescence

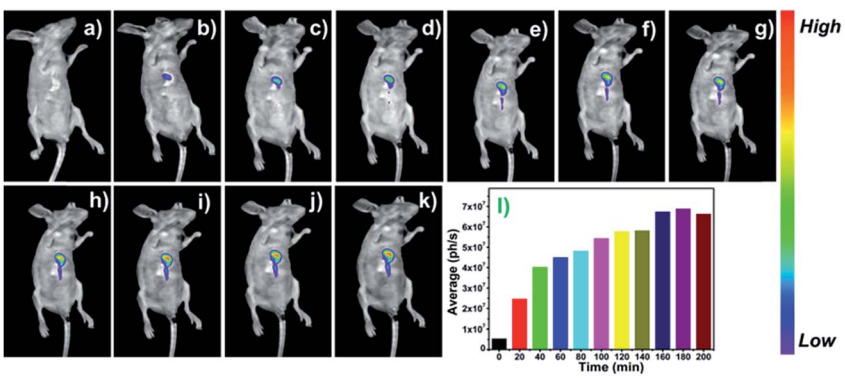

Fig. 8 Fluorescence imaging of APN activity in bare BABL/c mice bearing the HepG-2 xenograft tumour after being intratumorally injected with probe **DCM-APN** (100 μM, 150 μL). Fluorescence photographs (inset: (a) 0 min; (b) 20 min; (c) 40 min; (d) 60 min; (e) 80 min; (f) 100 min; (g) 120 min; (h) 140 min; (i) 160 min; (j) 180 min; (k) 200 min) were collected with 475 nm excitation (fwhm = 20 nm) and emission at 655 nm (fwhm = 20 nm). (l) The average (ph/s) was collected from the tumour site as a function of time.

signal using 800 nm of excitation. Based on the aforementioned results, we have verified the suitability of **DCM-APN** as the first NIR fluorescence probe for tracking APN endogenous activity in the tissue, which is useful for the early diagnosis and treatment of hepatocellular carcinoma in clinical practice.

Fluorescence imaging of APN activity *in vivo*

Encouraged by the outstanding performance in living cells, thereby, we explored the capability of probe **DCM-APN** for tracking the APN activity in mice bearing HepG-2 xenograft tumours. As depicted in Fig. 8, the bare BABL/c mice were intratumorally injected with the probe **DCM-APN** (100 μM, 150 μL). Using the NightOWL II LB983 small animal *in vivo* imaging system, an obvious fluorescence signal appeared at the tumour site *in situ* (Fig. 8b), with the fluorescence intensity gradually increasing as a function of time (Fig. 8b–k). Furthermore, the respective average fluorescence statistics (ph/s) are displayed in Fig. 8l, which were consistent with those of the fluorescence images. In contrast, a considerably weak fluorescence was obtained *via* subcutaneous injection without the HepG-2 xenograft tumour (Fig. S20†), which further confirmed that the probe could selectively light-up hepatocellular carcinoma with a high signal-to-noise ratio. By considering the above results, it was revealed that the probe **DCM-APN** exhibited potential to be employed for the early diagnosis and surgical imaging of hepatocellular carcinoma in clinical practice.

Conclusions

In summary, we have developed a novel two-photon NIR fluorescence probe **DCM-APN** for tracking endogenous APN activity in virtue of the regulation of the ICT mechanism. By specifically identifying the substrates (*i.e.*, a docking simulation), probe **DCM-APN** displayed high selectivity and ultra-sensitivity (DL 0.25 ng mL^{-1}) for APN. It was observed to be biocompatible, and could be employed to monitor the APN activity for distinguishing between cancer cells (*e.g.*, HepG-2 and B16/BL6 cells) and normal cells (LO2 cells). Notably, it was also used to investigate the APN activity at the hepatocellular carcinoma tissue using a one/two-photon confocal fluorescence microscope. Furthermore, a wound healing assay of tumour cells has demonstrated that APN plays an important role in cell migration. More importantly, HepG-2 xenograft tumour of mice is observed to be lit up through *in situ* injection with probe **DCM-APN**, thereby demonstrating that the probe shows potential to be used as an effective tool for the early diagnosis and evaluation of synergistic cancer therapies in clinical practice.

Conflicts of interest

The authors declare no competing financial interests.

Acknowledgements

This work was financially supported by the National Natural Science Foundation of China (21421005, 21576037, 21878039, 21822804 and 21676047), and NSFC-Liaoning United Fund (U1608222). All the animal procedures were performed in accordance with the Guidelines for Care and Use of Laboratory Animals of Dalian Medical University and experiments were approved by Dalian Medical University Animal Care and Use Committee.

Notes and references

1 L. Chen, Y. L. Lin, G. Peng and F. Li, *Proc. Natl. Acad. Sci. U. S. A.*, 2012, **109**, 17966–17971.
2 S. X. Cui, X. J. Qu, Z. H. Gao, Y. S. Zhang, X. F. Zhang, C. R. Zhao, W. F. Xu, Q. B. Li and J. X. Han, *Cancer Lett.*, 2010, **292**, 153–162.
3 J. S. Shim, J. H. Kim, H. Y. Cho, Y. N. Yum, S. H. Kim, H. J. Park, B. S. Shim, S. H. Choi and H. J. Kwon, *Chem. Biol.*, 2003, **10**, 695–704.
4 X. He, Y. Hu, W. Shi, X. Li and H. Ma, *Chem. Commun.*, 2017, **53**, 9438–9441.
5 Y. Aozuka, K. Koizumi, Y. Saitoh, Y. Ueda, H. Sakurai and I. Saiki, *Cancer Lett.*, 2004, **216**, 35–42.
6 R. Hata, H. Nonaka, Y. Takakusagi, K. Ichikawa and S. Sando, *Angew. Chem., Int. Ed.*, 2016, **55**, 1765–1768.
7 Y. Saitoh, K. Koizumi, T. Minami, K. Sekine, H. Sakurai and I. Saiki, *Biol. Pharm. Bull.*, 2006, **29**, 709–712.
8 M. Terauchi, H. Kajiyama, K. Shibata, K. Ino, A. Nawa, S. Mizutani and F. Kikkawa, *BMC Cancer*, 2007, **7**, 140.
9 P. Mina-Osorio, *Trends Mol. Med.*, 2008, **14**, 361–371.
10 N. Haraguchi, H. K. Ishii, F. Tanaka, M. Ohkuma, H. M. Kim, H. Akita, D. Takiuchi, H. Hatano, H. Nagano and G. F. Barnard, *J. Clin. Invest.*, 2010, **120**, 3326–3339.
11 A. M. Alizadeh, M. Sadeghizadeh, F. Najafi, S. K. Ardestani, V. Erfanimoghadam, M. Khaniki, A. Rezaei, M. Zamani, S. Khodayari and H. Khodayari, *BioMed Res. Int.*, 2015, **2015**, 824746.
12 M. Wickstrã, R. Larsson, P. Nygren and J. Gullbo, *Cancer Sci.*, 2011, **102**, 501–508.
13 D. Asanuma, M. Sakabe, M. Kamiya, K. Yamamoto, J. Hiratake, M. Ogawa, N. Kosaka, P. L. Choyke, T. Nagano, H. Kobayashi and Y. Urano, *Nat. Commun.*, 2015, **6**, 6463.
14 T. B. Ren, Q. L. Zhang, D. Su, X. X. Zhang, L. Yuan and X. B. Zhang, *Chem. Sci.*, 2018, **9**, 5461–5466.
15 D. Wu, L. Chen, N. Kwon and J. Yoon, *Chem*, 2016, **1**, 674–698.
16 J. Li, Y. Kwon, K. S. Chung, S. L. Chang, D. Lee, Y. Yue, J. Yoon, G. Kim, S. J. Nam and Y. W. Chung, *Theranostics*, 2018, **8**, 1411–1420.
17 K. Gu, Y. Xu, L. Hui, Z. Guo, S. Zhu, S. Zhu, S. Ping, T. D. James, T. He and W. H. Zhu, *J. Am. Chem. Soc.*, 2016, **138**, 5334–5340.
18 C. Zhao, X. Zhang, K. Li, S. Zhu, Z. Guo, L. Zhang, F. Wang, Q. Fei, S. Luo and P. Shi, *J. Am. Chem. Soc.*, 2015, **137**, 8490–8498.
19 A. Sharma, E. J. Kim, H. Shi, J. Y. Lee, B. G. Chung and J. S. Kim, *Biomaterials*, 2017, **155**, 145–151.
20 M. H. Lee, A. Sharma, M. J. Chang, J. Lee, S. Son, J. L. Sessler, C. Kang and J. S. Kim, *Chem. Soc. Rev.*, 2018, **47**, 28–52.

21 Z. Mao, M. Ye, W. Hu, X. Ye, Y. Wang, H. Zhang, C. Li and Z. Liu, *Chem. Sci.*, 2018, **9**, 6035–6040.
22 K. Gu, W. Qiu, Z. Guo, C. Yan, S. Zhu, D. Yao, P. Shi, H. Tian and W. H. Zhu, *Chem. Sci.*, 2018, DOI: 10.1039/c8sc04266g.
23 H. Li, Q. Yao, F. Xu, N. Xu, R. Duan, S. Long, J. Fan, J. Du, J. Wang and X. Peng, *Biomaterials*, 2018, **179**, 1–14.
24 R. J. Mellanby, J. I. Scott, I. Mair, A. Fernandez, L. Saul, J. Arlt, M. Moral and M. Vendrell, *Chem. Sci.*, 2018, **9**, 7261–7270.
25 Q. Miao, D. C. Yeo, C. Wiraja, J. Zhang, X. Ning, C. Xu and K. Pu, *Angew. Chem., Int. Ed.*, 2018, **57**, 1256–1260.
26 Y. Liu, L. Teng, L. Chen, H. Ma, H.-W. Liu and X.-B. Zhang, *Chem. Sci.*, 2018, **9**, 5347–5353.
27 W. Sun, J. Fan, C. Hu, J. Cao, H. Zhang, X. Xiong, J. Wang, S. Cui, S. Sun and X. Peng, *Chem. Commun.*, 2013, **49**, 3890–3892.
28 P. Liu, B. Li, C. Zhan, F. Zeng and S. Wu, *J. Mater. Chem. B*, 2017, **5**, 7538–7546.
29 H. Li, Q. Yao, J. Fan, J. Du, J. Wang and X. Peng, *Biosens. Bioelectron.*, 2017, **94**, 536–543.
30 A. Sedgwick, W. T. Dou, J. B. Jiao, L. Wu, G. T. Williams, A. T. A. Jenkins, S. D. Bull, J. L. Sessler, X. P. He and T. D. James, *J. Am. Chem. Soc.*, 2018, **140**, 14267–14271.
31 Y. Lv, D. Cheng, D. Su, M. Chen, B. C. Yin, L. Yuan and X. B. Zhang, *Chem. Sci.*, 2018, **9**, 7606–7613.
32 D. Cheng, Y. Pan, L. Wang, Z. Zeng, L. Yuan, X. Zhang and Y. T. Chang, *J. Am. Chem. Soc.*, 2017, **139**, 285–292.
33 L. Chen, W. Sun, J. Li, Z. Liu, Z. Ma, W. Zhang, L. Du, W. Xu, H. Fang and M. Li, *Org. Biomol. Chem.*, 2013, **11**, 378–382.
34 X. He, Y. Xu, W. Shi and H. Ma, *Anal. Chem.*, 2017, **89**, 3217–3221.
35 C. H. Tung, Q. Zeng, K. Shah, D. E. Kim, D. Schellingerhout and R. Weissleder, *Cancer Res.*, 2004, **64**, 1579–1583.
36 Z. Wang, W. Hao, P. Liu, Z. Fang and S. Wu, *Biomaterials*, 2017, **139**, 139–150.
37 K. Gu, Y. Liu, Z. Guo, C. Lian, C. Yan, P. Shi, H. Tian and W. H. Zhu, *ACS Appl. Mater. Interfaces*, 2016, **8**, 26622–26629.
38 M. Zeng, A. Shao, H. Li, Y. Tang, Q. Li, Z. Guo, C. Wu, Y. Cheng, H. Tian and W.-H. Zhu, *ACS Appl. Mater. Interfaces*, 2017, **9**, 13029–13036.
39 Y. Sato, *Biol. Pharm. Bull.*, 2004, **27**, 772–776.
40 K. Fukasawa, H. Fujii, Y. Saitoh, K. Koizumi, Y. Aozuka, K. Sekine, M. Yamada, I. Saiki and K. Nishikawa, *Cancer Lett.*, 2006, **243**, 135–143.